Polymerization of EDOT functionalized star-shaped pentaerythritol and study of the structure and conducting properties of polymers

Rana Abdel Samad, Frédéric Gohier, Barbara Daffos, Pierre-Louis Taberna, Charles Cougnon

ARTICLE

Polymerization of EDOT functionalized star-shaped pentaerythritol and study of the structure and conducting properties of polymers

Received 00th January 20xx,
Accepted 00th January 20xx

DOI: 10.1039/x0xx00000x

Rana Abdel Samad,[a] Frédéric Gohier,[a] Barbara Daffos,[b,c] Pierre-Louis Taberna[b,c] and Charles Cougnon*[a]

Conducting polymers (CPs) are undergoing a renewal in light of new challenges in energy storage posed by the environmental crisis through expanding their application to concepts of conducting redox polymers, nanostructured CPs and porous CPs. But if their conducting properties are widely documented, the same cannot be said for their structural properties, causing an increasing need of new solutions for the preparation of CPs with predetermined structures. In this study, we used a pentaerythritol core tertrafunctionalized with EDOT units as architectured monomer to prepare porous CPs with a controlled degree of openness and a hierarchical porous structure. Polymers were prepared by electrochemical and chemical oxidation of monomer solutions at different concentrations, and films were studied by cyclic voltammetry, quartz crystal microbalance, electrochemical impedance spectroscopy and gas sorption experiments. Results show that strong links exit between the porosity and the conductivity of films on the one hand, and the monomer concentration in the polymerization bath on the other, providing a simple way to control the textural and conducting properties of porous CPs.

1. Introduction

Since the early stage of research in energy storage, organic conducting polymers (CPs) are receiving special attention in both the academic and industrial communities, because of their inherent electrochemical, electrical and mechanical properties accounting for their very high capacitance and good processability. In this regard, it is of particular relevance to recall that the first batteries marketed at the end of the 80s are CPs-based; a few years before the marketing of the first Lithium-ion battery by Sony in 1991.[1] In these batteries, p-type CPs serve as cathode and lithium metal acts as anode. Unfortunately, the first CPs-based batteries encountered severe drawbacks and their commercialization was rapidly discontinued. Their major drawbacks are related to the conducting polymer it-self, which are partially oxidized (typical p-doping levels are comprised between 0.2 and 0.5 electron hole per monomer unit) to avoid irreversible degradation of CPs, and which suffer from a sloping voltage profile over the discharging period due to the potential dependence of the p-doping process.[2] As a result, CPs-based batteries were working far below their theoretical capacity and energy density. Today, in the urgency of the energy transition, CPs need to learn from their failures and research in this area is continuing to grow with the twin objective to improve their energy and power densities.[3] To reach these high objectives, physical and chemical methods were proposed to fabricate porous CP films with the potentiality to include attractive qualities for storage such as shortened pathways for ionic and electronic charge carriers, high mass and charge carrier mobilities, large electrochemically accessible surface, good stability and mechanical properties.[4-8] To date, there are many approaches to obtain porous CPs, which can be categorized as being template-based or template-free depending on whether their preparation is guided by a pre-nanostructured template or not.[9] Template-guided methods are the most popular approach because they are easily adaptable to all CPs, but precautions must be taken to avoid losing the inherent benefits offered by nanostructuration during the removal of the template. With a view of simplifying the procedure, template-free methods were proposed, among which the use of macromolecular or molecular porogens allowing a fine-tuning of the gap between the nanostructures of CPs.[10,11] In these solution-processed CP films, the morphology is guided by organic porogen additives in solution when the film is being formed. If termed as template-free method, the organic porogen is used as a sacrificial compound and must be subsequently removed. Noted that its elimination from the film remains energy-intensive or require large amount of solvents, goes against the principle of atom economy, quite

[a] Univ Angers, CNRS, MOLTECH-ANJOU, SFR MATRIX, F-49000 Angers, France. E-mail : charles.cougnon@univ-angers.fr
[b] CIRIMAT, Université de Toulouse III, Paul Sabatier.
[c] Réseau sur le Stockage Electrochimique de l'Energie (RS2E), FR CNRS 3459, 80039, Amiens Cedex, France.

†Electronic Supplementary Information (ESI) available. See DOI: 10.1039/x0xx00000x

apart from the fact that removing the porogen while keeping the nanostructured CP film intact remains challenging. In all cases, the vast majority of theses procedures fail to give hierarchical porous organic structures with controlled pore size distribution, which are increasingly relevant for specific applications such as chemical separation and storage, heterogeneous catalysis and energy storage.

The search for porous organic materials with controllable pore diameters and well-defined inner surface chemistry is the primary field of polymers of intrinsic porosity, which are envisaged as an ultimate solution to obtain uniform micropores in a single step. In this truly template-free approach, porous polymers are synthesized from monomers with shape-persistent 3D molecular architectures,[12] and textural properties arise from molecular cavities in the film, whose size and shape are directly controlled by generic molecular elements in the monomer.[13] For this application, macromolecules with extended rigid aromatic segments are powerful building blocks with the capability to produce polymers having a permanent porosity.[14,15] Microporous conducting polymers are particularly well suited to this approach due to their inherent extended pi-conjugated structure.[16,17] Most of these materials are prepared by repetitive metal-catalyzed homocoupling and crosscoupling reactions of aromatic subunits,[18] but more recently, they have also been obtained by oxidative chemical and electrochemical polymerization, especially for the preparation of high-performance organic materials in the field of energy storage.[19-23] In this area, physicochemical properties of the 3D electrolyte/polymer interface are crucial, because surface is the main entrance door to ions. Conducting polymers of intrinsic porosity offer a unique opportunity to control both the morphology and surface chemistry by modulating the building block chemistry to correct severe drawbacks of CPs, such as polymer fatigue due to volumetric swelling and shrinkage during redox switching, mechanical rigidity of the polymer backbone by introducing flexible segments for improving its adhesion towards current collectors and active particles for the preparation of binder-free electrodes, and reversible change in surface wettability that in turn impacts ion accessibility in polymers.[24-26] Here we report the synthesis and electrochemical study of a 3,4-ethylene-dioxythiophene (EDOT) functionalized star-shaped monomer using a pentaerythritol core as new building block for the preparation of a conductive polymer of intrinsic porosity. Because of its high molecular symmetry, its flexibility and its four equivalent alcohol groups, pentaerythritol is often used as raw material for the preparation of dendritic-like organic structures with the extremely specific architectural and chemical requirements necessary for the development of intrinsic microporous and hypercrosslinked materials enriched with oxygen.[27-30] These materials have potential for applications requiring porosity, flexibility, stability and specific surface chemistry, and are considered as promising adsorbents for gas separation and storage.[31-33] More recently, they have been tested in flexible electronics, electrochemical energy storage and opto-electronics.[34-38] But to the best of our knowledge, apart from the work of U. Bulut et al. on pentaerythritol end-functionalized with four thiophene groups, who found that no electropolymerization takes place under their conditions, no research was reported on conducting polymers with pentaerythritol core units.[39] However, the possibility for the polymerization of pentaerythritol-based monomers open new avenues for moving conducting polymers beyond their traditional scope of application so far mainly focused on their electronic conducting properties.

The purpose of this work is to clarify the experimental conditions under which the EDOT functionalized pentaerythritol polymerizes, and to study the impact of these conditions on the quality of films prepared by electrochemical and chemical oxidation. Cyclic voltammetry, electrochemical impedance spectroscopy, quartz crystal microbalance and gas sorption experiments demonstrate that strong links exist between the texture and the conductivity of films on the one hand, and monomer concentration in the polymerization bath on the other.

2. Experimental

2.1 Instrumentations and Procedure

Electrochemical experiments were made in a three-electrode cell containing dichloromethane (DCM) + 0.1 M nBu_4NPF_6. The counter electrode was a platinum wire and the working electrode was a glassy carbon electrode (3 mm in diameter). The working electrode was mirror polished and sonicated for 5 min in DCM before analysis. All potential values were referred to the $Ag/AgNO_3$ system. A bipotentiostat from CH Instruments (model 920C) and a VMP-Biologic potentiostat (model SP-150) were used. Microgravimetric measurements were performed by using ATcut 9MHz gold-coated quartz crystal oscillators connected to a PAR quartz crystal analyser model QCM922 driven by the EC-Lab software (version 11.52). For impedance measurements, the amplitude of the ac signal was 5 mV and the frequency varied between 500 kHz and 1 mHz. Nitrogen adsorption–desorption isotherms were measured at 77K using Micromeritics ASAP 2020. The Brunauer–Emmett–Teller (BET) equation was used to calculate the specific surface area (SSA). The pore size distribution (PSD) was calculated from adsorption isotherms using a 2D non-local density functional theory (2D-NLDFT) model based on Saeius software from Micromeritics.

2.2 Synthesis of EDOT functionalized pentaerythritol

The EDOT functionalized pentaerythritol was synthesized by copper(I)-catalyzed 1,3-dipolar cycloaddition (click chemistry) between compounds **1** and **2** (Scheme 1). Full synthetic details may be found in ESI† (Fig. S1, S2, S3 and S4).

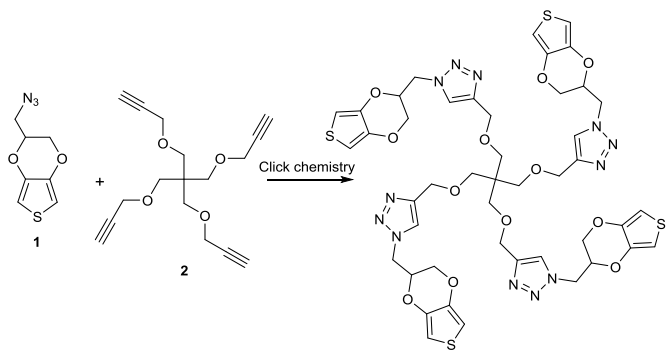

Scheme 1 Synthesis of EDOT functionalized pentaerythritol

2.3 Electrochemical and chemical preparation of polymers

Polymers were prepared by electrochemical oxidation of monomers via cyclic voltammetry in DCM + 0.1 M Bu_4NPF_6, and by oxidative chemical polymerization, using $FeCl_3$ in excess in a deaerated solvent mixture of DCM/ACN at room temperature. Noted that for the electrochemical polymerization, the potential window utilized was selected in such a way that the monomer is oxidized and the film is neutralized at each cyclic voltammogram. Full synthetic details can be found in ESI†. FT-IR spectra of the synthesized EDOT-functionalized pentaerythritol monomer, PEDOT and pentaerythritol-based films were acquired to identified the main chemical functionalities in the polymer products as shown in Fig. S5.

3. Results and discussion

3.1 Effect of the monomer concentration on the electrochemical polymerization

Since it was reported in literature that no polymer is obtained by electrochemical oxidation of thiophene functionalized pentaerythritol,[39] we first explore the specific conditions in which our parent molecule electropolymerizes. As a starting point, the effect of the monomer concentration in the polymerization bath was investigated by cyclic voltammetry. Fig. 1a-e show series of consecutive cyclic voltammograms (CVs) obtained at different monomer concentrations. In all cases, during the first CV a large irreversible anodic current is obtained from 1 V vs. $Ag/AgNO_3$ that is due to the four equivalent EDOT groups per monomer. But for the subsequent CVs the evolution of the current appears strongly impacted by the monomer concentration. For concentrations higher than 0.5 mM (Fig. 1a and b), the current ascribed to the oxidation of the monomer decreased as the number of CV increased, giving no faradaic current over the whole potential domain cycled for a concentration of 2 mM, and producing the emergence of a resistive p-doping process at 1 mM. On the contrary, when the monomer concentration became lower than 1 mM (Fig. 1c-e), repetitive CVs shown a progressive current increase over a large potential domain that is typically obtained for the formation of organic semiconducting films on the electrode surface. Remarkably, the potential domain over which the current grows is expanding towards negative potentials as the monomer concentration decreased, corresponding to an increasingly low p-doping onset potential that is expected for extended conjugation lengths in films. It results to the above that films of different qualities were obtained depending on the monomer concentration. Noted that the absence of electropolymerization at the highest monomer concentration (Fig. 1a) is consistent with the previous study reported by U. Bulut et al. who concluded that a 10 mM solution of a parent four-armed thiophene compound reveals no electropolymerization activity.[39]

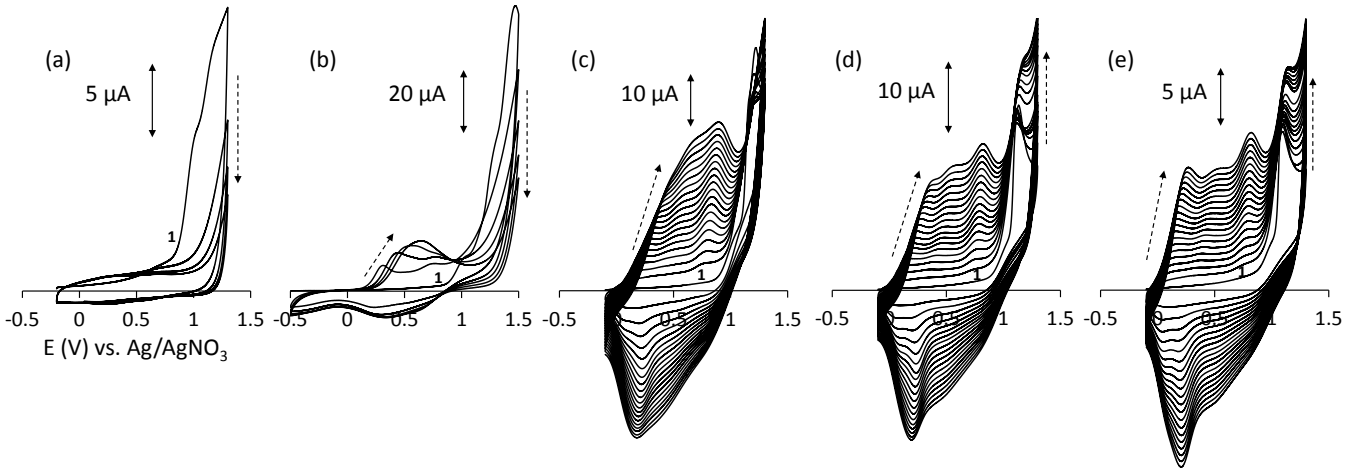

Fig. 1 Cyclic voltammograms recorded at 100 mV s^{-1} on glassy carbon (GC) electrodes in dichloromethane (DCM) + 0.1 M Bu_4NPF_6 containing 2 mM (a), 1 mM (b), 0.5 mM (c), 0.25 mM (d) and 0.125 mM (e) of EDOT functionalized pentaerythritol

Interestingly, after four repetitive CVs in a 2 mM solution of monomer, the electrode surface was totally blocked towards electron transfer compared to the electrochemical response of a bare glassy carbon electrode, as demonstrated by the CV of the ferri/ferrocyanide couple (2 mM) in 0.1M KCl aqueous solution (Fig. 2a). This is evidence for the formation of an insulating film that passivates the electrode surface. In the same way, after repetitive CVs in a 0.125 mM solution of monomer, the electrode shows a diode-like behaviour towards ferri/ferrocyanide as just an irreversible anodic wave is obtained in 0.1M KCl containing 2 mM $Fe(CN)_6^{-3/-4}$ (Fig. 2b).[40,41] For demonstration purposes, the CV of the p-doping process of the film is superimposed in Fig. 2b (long-dashed curve). The fact that the anodic wave attributed to the oxidation of the redox probe has slightly moved towards positive potentials to coincide with the p-doping onset potential indicates the semiconducting nature of the film obtained at low monomer concentration.

The concentration effect reported above can be tentatively rationalized as a result of intermolecular and intramolecular oxidative coupling products during electropolymerization, as it is well-known that the concentration of a substrate allows to control selectivity towards either inter or intramolecular coupling reactions. In this perspective, dilution of monomer is expected to promote intramolecular coupling, which has the consequence of decreasing the degrees of freedom associated with the star-shaped monomer.

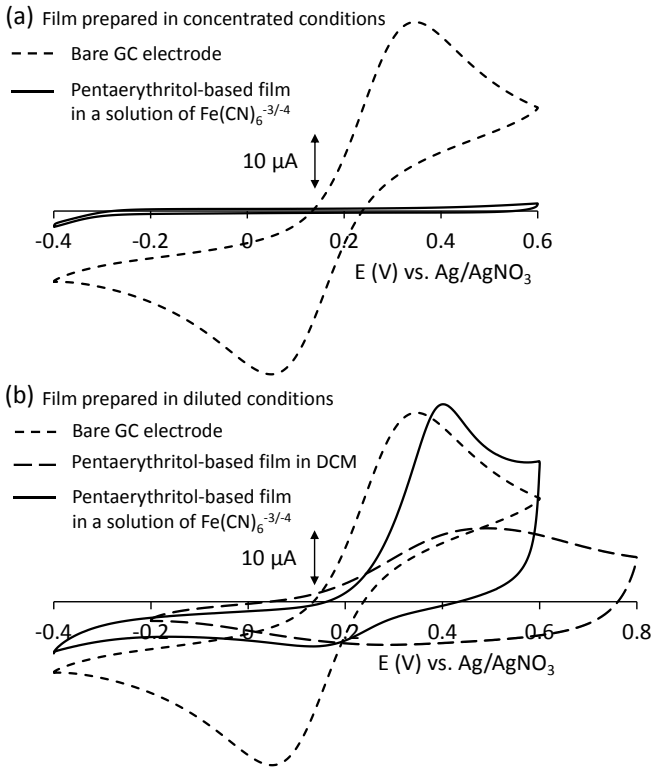

Fig. 2 Cyclic voltammograms in solid lines are recorded at 100 mV s^{-1} in 0.1 M KCl containing 2 mM $Fe(CN)_6^{-3/-4}$ on GC electrodes previously cycled in DCM solutions containing 2 mM (a) and 0.125 mM (b) of pentaerythritol-based monomer, as shown in Fig. 1a and e. Noted that CV in short-dashed line is obtained with a freshly polished GC electrode, and CV in long-dashed line corresponds to the response of the film in DCM + 0.1 M Bu_4NPF_6.

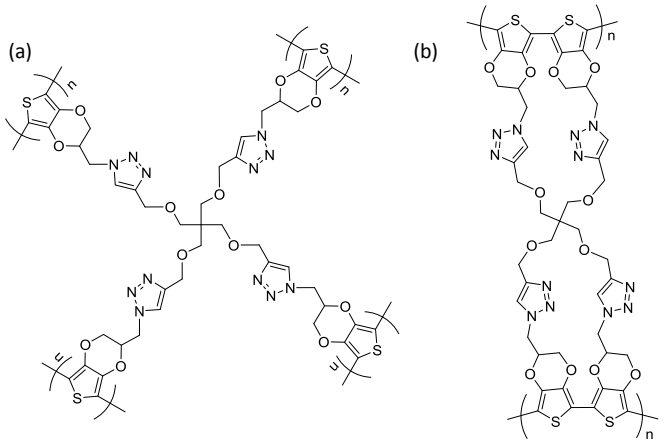

Scheme 2 Schematic representation of (a) pure inter-molecular polymerization and (b) pure intra-molecular polymerization of EDOT functionalized pentaerythritol monomer.

Scheme 2 illustrates the two extreme cases corresponding to pure intermolecular polymerization (scheme 2a) for highly concentrated monomer solutions, and pure intramolecular polymerization for highly diluted monomer solutions (scheme 2b). The former conditions are expected to give films with a dendritic structure, while the latter give a more compact semiconducting polymer. In realistic conditions, a mixed inter-intramolecular polymerization mechanism is most likely to

occurs, making the conducting and morphological properties of films very sensitive to the monomer concentration.

3.2 Effect of the monomer structure and concentration on textural properties of films

Nitrogen adsorption-desorption experiments. It results to the above that the monomer concentration is expected to have a strong impact on the degree of openness of the polymer network, giving variations in the porosity of films. In this perspective, gas sorption measurements were made to obtain information on the textural properties of films produced by chemical oxidative polymerization of 0.05 mM and 0.5 mM solutions of monomer by using $FeCl_3$ as oxidant. Results were compared to a PEDOT film synthesized in the same conditions to examine the impact of the pentaerythritol core on the structure of films. Fig. 3a shows the pore size distribution (PSD) of PEDOT and pentaerythritol-based polymers, and Fig. 3b shows their cumulated surface areas. Remarkably, pentaerythritol-based films present a hierarchical porous structure revealing three pore size populations, while the PSD for PEDOT covers a continuous pore size distribution ranging from 1.5 nm to 30 nm. As it is well-known that porosity of PEDOT consists in the interstitial void between polymer chains and fibers,[42] it can be reasonably anticipated that the discrete pore size distribution obtained with pentaerythritol-based films corresponds to the size of generic structural elements in the monomer, especially for the two smaller pore size populations which are compatible with the dimensions of molecular cavities resulting from intra and intermolecular polymerization of the pentaerythritol-based monomer. Importantly, the smallest pore size population at around 0.45 nm fit well with interatomic distances calculated by Chem3D inside the small cavity produced by intramolecular coupling (scheme 2b), while the pore size population at around 1.5 nm may be ascribed to the dimensions of cavities obtained by intermolecular polymerization. Noted that the largest pore size population at ca. 20 nm in diameter may be attributed to the interstitial space between polymer fibers as it is also obtained with PEDOT. As a result, the discrete pore size populations for pentaerythritol-based films taken in ascending order of their diameter are hereinafter referred to as “intra-cavity”, “inter-cavity” and “interstitial cavity”. Interestingly, for the pentaerythritol-based film obtained in the more concentrated conditions, pores corresponding to “intra-cavity” are not visible on the PSD, causing an increase in the average pore diameter from 7.8 nm to 12.3 nm when the concentration of the pentaerythritol-based monomer in the polymerization bath changes from 0.05 mM to 0.5 mM. At the same time, the BET surface of the film increases from 2.8 $m^2 g^{-1}$ to 31 $m^2 g^{-1}$.

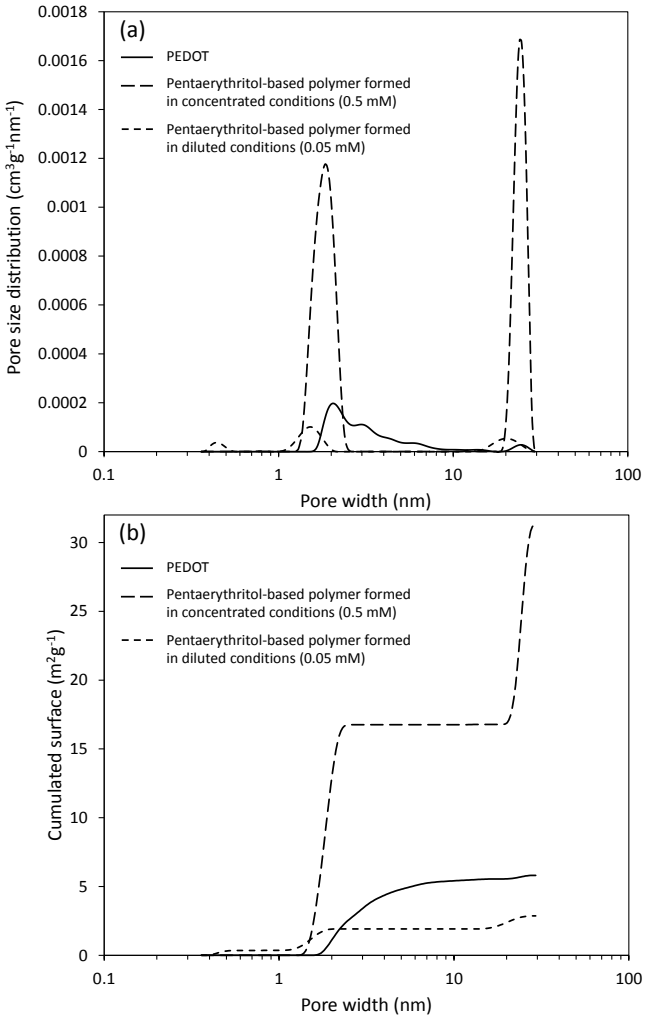

Fig. 3 Nitrogen adsorption/desorption study of PEDOT (solid line) and pentaerythritol-based films produced by chemical oxidative polymerization of 0.05 mM (short-dashed line) and 0.5 mM (long-dashed line) solutions of monomer. (a) Pore size distribution and (b) surface cumulated areas.

These results are fully consistent with the concentration-dependent polymerization mechanism postulated above where intramolecular coupling are dominant at low monomer concentration, giving small cavities in a more compact polymer, while an increase of the monomer concentration promotes the intermolecular coupling, yielding a dendritic-like polymer with large cavities and a higher degree of openness. Remarkably, starting from a 0.5 mM solution of the pentaerythritol-based monomer, the film shows a unimodal PSD, if we except the interstitial cavities.

Quartz crystal microbalance study of films. Quartz crystal microbalance is widely used to study the morphological changes in conducting polymers. Especially, it is well known that free solvent molecules captured inside the film during its formation and exchanged during the p-doping process give a valuable indication on the free volume inside the film.[43,44] Quartz crystal microbalance combined with cyclic voltammetry shown that the potential dependence of the solvent flux is

non-monotonic, because counter anion exchange and morphological change of the film affect the solvent transfer differently.[45] Typical cyclic massogram of PEDOT and films prepared by electrochemical oxidation of 0.05 mM, 0.25 mM and 0.5 mM solutions of pentaerythritol-based monomer are shown in Fig. 4a as a function of potential, and in Fig. 4b as a function of charge doping. The non-monotonic change in mass during the oxidation of PEDOT is particularly clear in Fig. 4b where the slopes of the different linear portions of the curve allow to calculate the apparent exchanged molar mass, $\boldsymbol{M_{app}}$, envisioned as the sum of the molar masses of the anion $\boldsymbol{M_{anion}}$ and the solvent $\boldsymbol{M_{solv}}$ (as it is well known that the cation exchange is absent for PEDOT)[46] :

$$M_{app} = M_{anion} + \alpha M_{solv}$$

Where α the number of solvent molecules transferred per anion between the film and the electrolyte. Noted that a negative value of α indicates that the fluxes of solvent and anions are in opposite directions. The values of α are shown in Fig. 4b for PEDOT and for pentaerythritol-based films. For PEDOT, results are in good agreement with the previous results reported in literature for other solvents,[43-45] and demonstrate that i) one molecule of solvent is replaced by one anion in the low charge doping domain, ii) the injection of ions in the film at intermediate doping levels is accompanied by the entrance of molecules of solvent in an equimolar amount, and iii) the mass increase at high doping levels is consistent with the entrance of ions alone. Assuming that the molecular volume of dichloromethane is very close to that of PF_6^-, the solvent-exclusion mode observed at the beginning of the p-doping process of the PEDOT reinforces the idea that the film has a rigid structure in neutral and low oxidation states.[43] In contrary, the inclusion of solvent molecules with counter anions at intermediate doping states was ascribed to conformational changes in the PEDOT film produced by creation of double bonds and electrostatic repulsion between polymer chains, creating void spaces in the film so that solvent molecules may go back into the film. In a fully open conformational state (i.e. at high p-doping level), the apparent mass exchange is as if counter anions enter alone inside the film.

Remarkably, Fig. 4b demonstrate that monotonic mass changes are obtained with pentaerythritol-based films throughout the entire charge doping range investigated, corresponding to a different doping dynamic. In all cases, constant and negative values for α suggest that the incorporation of anion dopants is controlled by the exclusion of solvent molecules whatever the doping level is. This means that films behave as rigid molecular structures with no change in degree of openness over the p-doping process (i.e. no polymer chain relaxation). This can be seen as a direct result of hyper-crosslinking between four-armed EDOT-based monomers resulting in a 3D continuous porous organic framework. Interestingly, results in Fig. 4b show that the number of molecules of solvent excluded per anion in the electrochemical doping process of films increases as the concentration in monomer used for their preparation

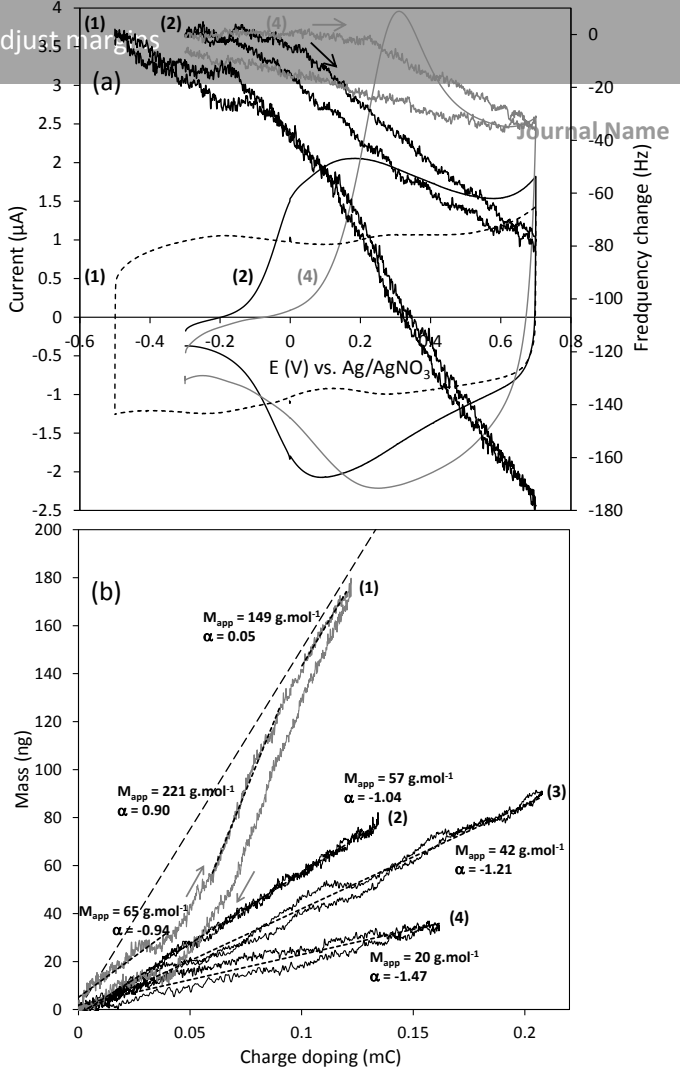

Fig. 4 EQCM study of PEDOT (curve 1) and pentaerythritol-based films produced by electrochemical oxidation of 0.05 mM (2), 0.25 mM (3) and 0.5 mM (4) solutions of monomer. (a) Cyclic voltammograms at 10 mV s^{-1} in DCM + 0.1 M Bu_4NPF_6 with frequency change as a function of potential. (b) Massograms as a function of the p-doping charge of films.

increases. This is probably because a most solvated film is obtained from a more concentrated solution of monomer, which is consistent with nitrogen adsorption-desorption experiments showing that the average pore diameter increases when the monomer concentration in the polymerization bath increases.

Cyclic voltammetry study of films. The rigid open framework structure mentioned above is expected to have a profound impact on the electrochemical behaviour of the film, as it is widely recognized in the scientific literature that the redox switching of a conducting polymer is strongly coupled to conformational changes.[47,48] In the electrochemically stimulated conformational relaxation (ESCR) model, these conformational changes are considered to be electrochemically induced.[49-53] In this model, thoroughly exemplified by studies of polypyrrole and PEDOT films, the dominant pathways for structural changes are geometrical reorganization of the polymer chain network by electrochemical production of polarons and bipolarons during oxidation and Coulombic repulsion between them, while conversely, polymer chains collapse inwards in undoped state, giving a more compact film. These conformational changes are magnified when the film is more reduced at the start of the p-

doping process, causing a change in the shape of the CV and making the cyclic voltammetry sensitive to the pre-polarization conditions.[54] For PEDOT, a holding of the initial potential where the film is under neutral state produces a shift of the p-doping process towards positive potentials because an additional amount of energy is required to open the polymer network, which is supplied by the anodic overpotential (Fig. S6). This potential dependence of the CV is an indication that redox kinetics and structural changes occur in tandem, both related to the thermodynamic state of the film.

Fig. 5a and 5b present CVs recorded on polymer films prepared by electrochemical oxidation of 0.5 mM and 0.05 mM solutions of pentaerythritol-based monomer. Still with the idea of studying the impact of the pre-polarization conditions on the redox switching in polymers, the initial potential is hold at -1 V during different times before to start the CV, and Fig. S7 and S8 present CVs obtained for the same films by starting the potential sweep from different initial potentials. Insets of Fig. 5a and 5b show the chronoamperometric responses of films stepped from -1.5 V and -2 V vs. $Ag/AgNO_3$ to the same anodic potential (0.4V). Noted that these experiments were achieved in a glove box. For the film obtained with the most concentrated solution, the forward scan of the CV consists in a well-defined anodic peak located at ca. 0.1 V, followed by a plateau current (Fig. 5a). As the initial potential was holding for a longer time, the anodic peak becomes higher in current intensity, but no shift in potential was obtained. This implies that during oxidation, the energy required to switch the film from the insulating to the conducting state stays the same when the film is more reduced, proving that the film remains under the same thermodynamic state whatever its neutralization status that is consistent with a rigid framework structure produced by hyper-crosslinking between four-armed EDOT-based monomers.

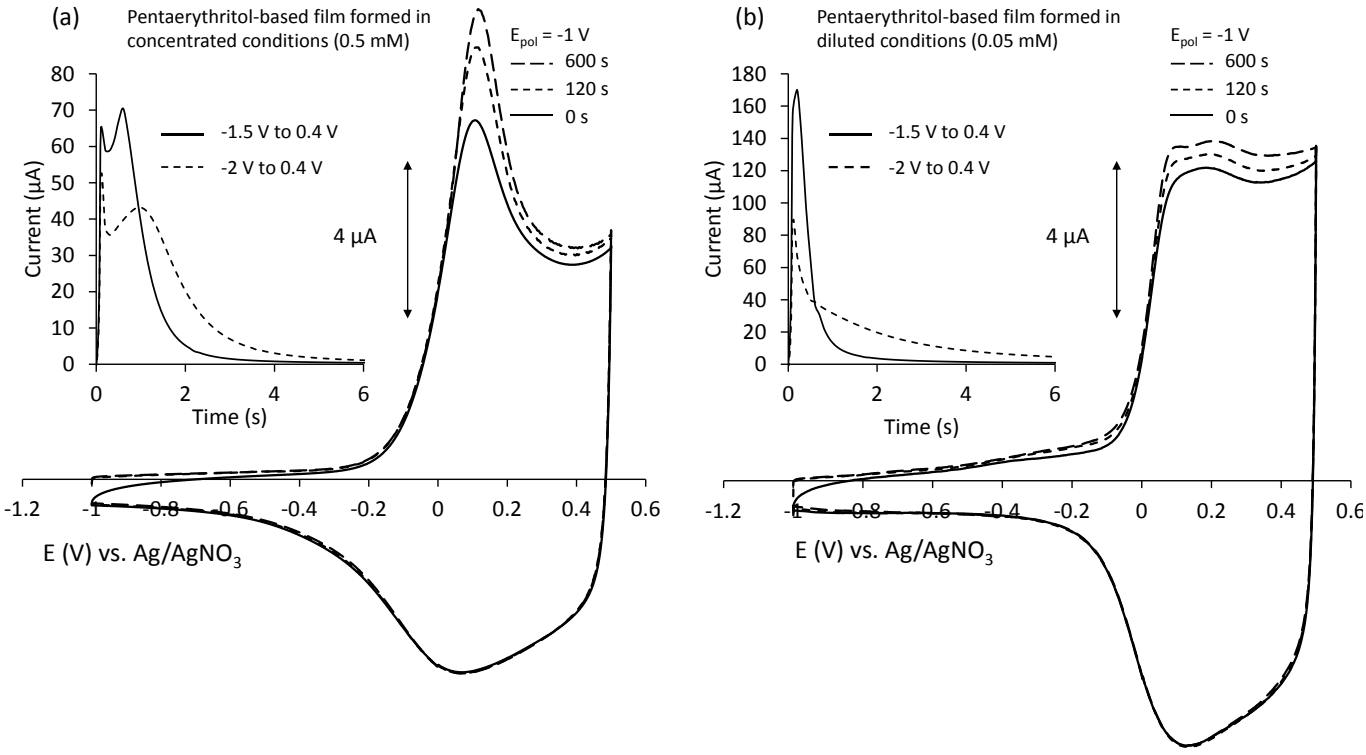

Fig. 5 Cyclic voltammograms recorded at 50 mV s^{-1} in DCM + 0.1 M Bu_4NPF_6 on GC electrodes covered with films after polarization at -1 V for 0 s , 120 s and 600 s. Insets show chronoamperometric responses of films stepped from -1.5 V (solid line) and -2 V (dotted line) for 120 s to 0.4 V. Films were previously prepared by electrochemical oxidation of 0.5 mM (a) and 0.05 mM (b) solutions of pentaerythritol-based monomer in DCM + 0.1 M Bu_4NPF_6 by consuming a polymerization charge of 1.05 mC in both cases.

Interestingly, during the neutralization process (in the backward scan), the shape of the CV does not changes with the different pre-polarization conditions, and the cathodic current gradually decreases without becoming equal to zero, even at very negative potentials, causing a current-potential hysteresis loop for the doping-dedoping process.[55] This implies that, in the backward scan, the conductivity of the film switch from “on” state to “off” state before the neutralization is complete, so it has become difficult for counterions to find a “way” across the film towards the electrolyte. It results that the entire doping-dedoping cycle depicted in Fig. 5a is evidence for a transition between two different regimes for ion transport, changing from one to another by modulating the charge doping. Chronoamperometric responses presented in inset of Fig. 5a allow a better understanding of these two regimes. After a sharp initial current maximum due to the electrochemical double-layer charging at the polymer-electrolyte interface, the broader current peak obtained is strongly reminiscent of a nucleation phenomenon, implying

that the oxidation of the film is initiated at local levels, before propagating throughout the film.[49-53]

Phenomenologically, right after the double-layer charging, the progressive current increase in the earlier stages of the oxidation corresponds to the creation of local conductive domains inside the film, envisioned as nuclei, followed by their growing in size, and ultimately, by their overlapping at the current maximum, corresponding to the fully conductive film. The Cottrell-like decay in current that follows is evidence for a diffusion-controlled mass transport or, more adequately, electric-field-induced migration of non-electroactive doping agents in deep oxidized films, implying that the counter-ion motion inside the polymer film is then totally decoupled to the short-time transient conduction regime.

When the film was prepared from a more diluted solution of the monomer, Fig. 5b indicates that the p-doping process remains relatively insensitive to the pre-polarization conditions. CVs obtained by holding the initial potential for long times or by starting the potential sweep from a more negative initial potential (Fig. S7), show a slight increase of the anodic current and no shift in potential. Again, absence of anodic overpotential after neutralization during a longer period indicates that there is no conformational change during the redox switching of the film, as expected for a rigid reticular organic framework. The only difference with CVs in Fig. 5a is that a more symmetrical pair of cathodic and anodic waves is obtained, reflecting a faster redox switching that agrees well with the formation of longer conjugated segments in the film by intramolecular polymerization. Importantly, chronoamperometric experiments presented in the inset of Fig. 5b prove that there is a different dynamic for the p-doping process, because no nucleation phenomenon is obtained in these conditions. Here, the incorporation of ions during oxidation is controlled by diffusion and/or electromigration at the start of the oxidation step, displaying a Cottrell-type decay of the anodic current immediately after the double-layer charging. In these conditions, the absence of current transient of nucleation for the doping process indicates there is no local space charge formation in the film, leading directly to a homogeneously electrified film. Such transition from heterogeneous to homogeneous charge distribution as the monomer concentration decreases in the polymerization bath may be regarded as a direct consequence of the relative importance of the inter and intramolecular polymerizations. In this model, a more concentrated monomer solution promotes the intermolecular polymerization producing a dendritic-like polymer with short coupling products behaving as spatially fixed redox centers capable of guaranteeing the redox conductivity by the electron hopping mechanism.[56-60] On the contrary, a more diluted monomer solution promotes the intramolecular polymerization, producing a more compact conducting polymer with longer effective conjugation lengths that makes possible the formation of polaron upon charge injection. In a more realistic way, a mixed inter- and intramolecular polymerization mechanism could produce coupling products with a large distribution of the effective conjugation length, the longest of which are expected to drive the conductivity to increase.[61] In this conceptual representation, it may be anticipated that the current transient of nucleation observed during the p-doping of the film obtained with a more concentrated solution of the monomer probably results to a mixed conduction effect combining "metallic" and "non-metallic" redox sites. Phenomenologically, it may be understood as a doping process locally driven at the level of "metallic" redox sites in the film, followed by diffusive propagation of the charge in the film by electron hopping between immobilized "non-metallic" redox centers, identified to the shortest effective conjugation lengths in the film (scheme 3).

Electrochemical impedance spectroscopy study of films. EIS is a powerful tool to have a full understanding of the electron and ion dynamics at electrochemical interfaces since it allows the deconvolution of physico-chemical phenomena occurring at different timescales just by measurements over a wide frequency range.[62] Most often conducting polymers may be envisioned as a two-carrier system behaving as an ideal selectively blocking electrode (i.e. blocking for ions and reversible for electrons). In these situations, the impedance response in the complex plane over a wide frequency range typically shows a semi-circle in the high frequency domain, ascribed to the electron transfer at the interface, a classical Warburg impedance visible as a 45° line, interpreted as ion diffusion or migration in the film, and a vertical line at low frequency due to the blocking boundary condition for mobile ions at the end of the diffusion domain.[63,64] Impedance data for a PEDOT film (used for reference) and for films prepared by electrochemical oxidation of 0.05 mM and 0.5 mM solutions of pentaerythritol-based monomer are shown in the complex plane representation in Fig. 6. Noted that impedance measurements are achieved at 0.1 V in DCM + 0.1 M Bu_4NPF_6.

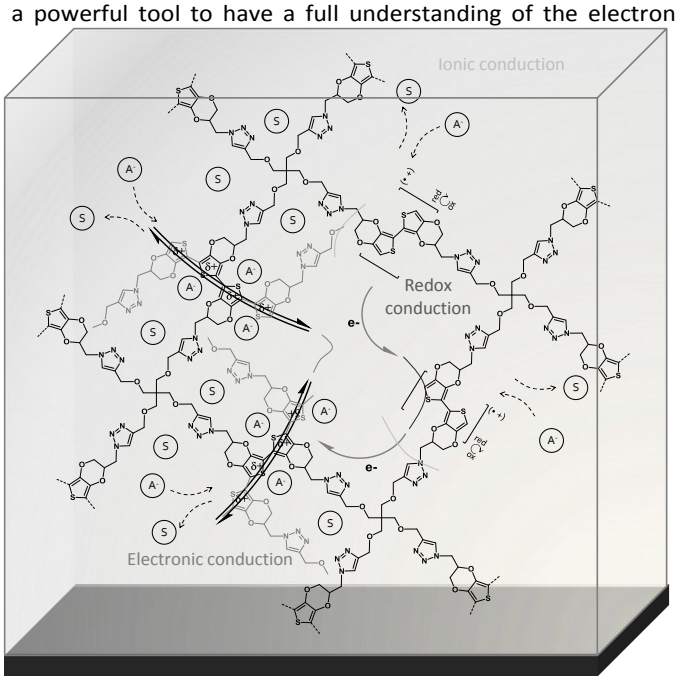

Scheme 3 Representation of the structure and conducting properties of the EDOT functionalized pentaerythritol-based polymer. In this representation, counter anions and molecules of solvent are denoted by A^- and S.

At this potential, the electronic conductivity of PEDOT is high compared to its ionic conductivity, so that the Warburg-type region is not visible (see Fig. 6, open triangles).[65] For the two other pentaerythritol-based films, the dc resistance at the lowest frequency (the total electronic resistance) increases as the monomer concentration in the polymerization bath increases, in accordance with the poorer electrochemical reversibility for the redox switching observed in Fig. 5a. Noted that, in all cases, impedance responses are moving towards vertical lines in the low frequency limit, which attest to a capacitive behaviour when the diffusion is complete, in accordance with a rapid shutdown for the charging current in chronoamperometric measurements presented in Fig. 5. It is confirmation that the electrode/film interface acts as a blocking surface for ions at low frequencies.

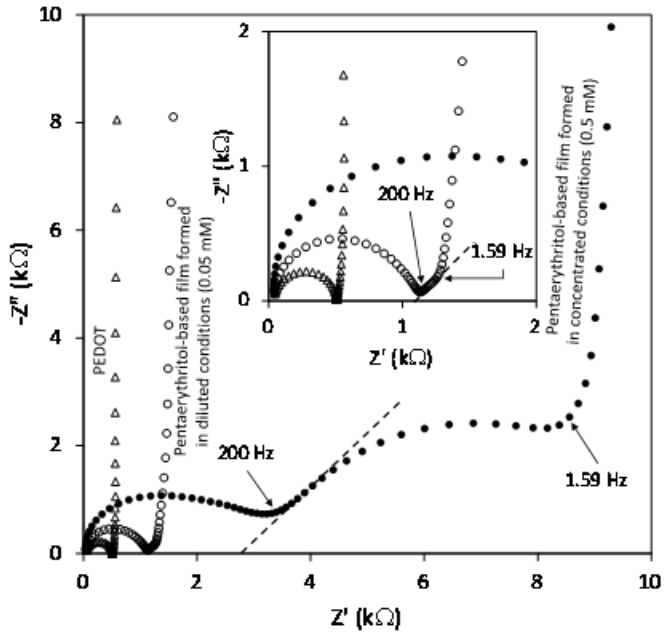

Fig. 2 Nyquist plots of the impedance of a PEDOT film (open triangles) and of films prepared by electrochemical oxidation of 0.05 mM (open circles) and 0.5 mM (solid circles) solutions of the pentaerythritol-based monomer. Impedance measurements were achieved at 0.1 V in DCM + 0.1 M Bu_4NPF_6 and films were prepared by consuming polymerization charges of 1.1 mC. The graph in inset shows the magnification of the high frequency part of the impedance plots.

Interestingly, for pentaerythritol-based films, an intermediate frequency regime appears as a 45° linear branch or an arced curve for the total impedance. This is also an indication that the electronic conductivity of pentaerythritol-based polymers is less than that of PEDOT, thus becoming sensitive to the a.c. potential perturbation in the intermediate frequency domain, ranging from approximately 200 Hz to 1.59 Hz. Importantly, in the high limit of the intermediate frequency domain, the classical Warburg response is obtained for the two pentaerythritol-based films, as highlighted by the 45° tilted dotted lines in Fig. 6. This is because at these frequencies the diffusion length of ions, which is frequency-dependent, is very small relative to the thickness of the finite diffusion region, so that the diffusion process is not affected by the boundary condition at the end of the diffusion zone. When the frequency approaches the low limit of the intermediate frequency domain (i.e. when the diffusion length of ions is no longer negligible compared to the size of the diffusion zone), a very different situation appears for the pentaerythritol-based film obtained in the more concentrated conditions. In this case, a depressed semi-circle appears instead of a 45° line, implying that the diffusion impedance is becoming more resistive in nature as the frequency decreases. Such arced impedance starting with a 45° line and inserted between the high frequency semi-circle and the low frequency vertical line may refer to a non-conventional Warburg impedance. At this stage, it is important to bear in mind that there is abundant literature on such non-classical diffusion impedances, because the Warburg impedance is based on a set of standard conditions often ill-suited in real cases, so that strong deviations from the classical Warburg impedance can be obtained by releasing only one of the assumptions stated in the original Warburg impedance model.[66] In ESI†, we reviewed the main models used to discuss these deviations and we present arguments for and against these models regarding our results.

Here, we argue that the 45° lines in the high frequency limit of the diffusion impedances visible in Fig. 6 for pentaerythritol-based films provided evidence for Fickian diffusion processes. This implies that the nucleation phenomenon corresponding to the charge propagation from nuclei, identified as polaron acting as charged point-sources for the p-doping process, towards the rest of the film, identified as a finite diffusion domain, may be regarded as a diffusive electron hopping between redox centers in the film.[56-60] In such a configuration, the diffusion is expected to occur in a spherical symmetry, in good accordance with the arced Warburg impedance theorized by Jacobsen and West in the spherical case.[66,67] Noted that, in the high frequency limit of the diffusion impedance, the diffusion length of ions is so small compared to the size of the finite-length diffusion domain that the a.c. potential perturbation is not sensitive to the geometry of the diffusion process, moving towards the 45° line typically obtained for the Warburg impedance in planar symmetry. These changes in conducting properties of the film, depending on whether the polymer was obtained from a diluted or a concentrated monomer solution, were attributed to the possibility of inter and intramolecular coupling of EDOT units in the pentaerythritol-based monomer, implying that such concentration effect should disappears by suppressing the intramolecular coupling with bulky polymerizable units at the four ends of the pentaerythritol branches. This last assumption will soon be verified in a forthcoming publication.

4. Conclusion

This work reports on the first successful polymerization of a pentaerythritol monomer functionalized at the four ends with an aromatic electropolymerizable unit. Results show a strong effect of the monomer concentration on the structure and conducting properties of films obtained either by

electrochemical and chemical oxidative polymerization. It was alleged that this effect may be due to the possibility of inter and intramolecular polymerization, giving a dendritic-like polymer in concentrated conditions or a more compact polymer in diluted conditions. BET experiments demonstrate that the degree of openness of the polymer network may be controlled by the monomer concentration in the polarization bath, yielding a hierarchical porous organic structure revealing discrete pore size populations whose dimensions are imposed by the size of generic elements in the monomer. In diluted conditions, a conducting polymer of intrinsic porosity characterized by a single pore population was obtained. More interestingly, because of the shape-persistent macromolecular structure of the monomer in the microporous architecture of the polymer, this approach allows potentially to modulate the porosity at the nanoscale by changing the size of generic molecular elements in the functionalized pentaerythritol core. Quartz crystal microbalance and cyclic voltammetry experiments give evidence that pentaerythritol-based films may be regarded as a rigid polymer framework produced by hyper-crosslinking of pentaerythritol-based monomers. Double potential step chronoamperometry between neutral and p-doped states and electrochemical impedance show that the p-doping current of pentaerythritol-based films is transitioned from a Cottrell-type decay to a nucleation growth when the monomer concentration increases in the polymerization bath. All the results obtained demonstrate that the pentaerythritol core can offer new possibilities to easily prepare oxygen-enriched 3D organic semiconducting materials in one step.

Author Contributions

C. C. took part in developing the concept and structuring of the project and experimental approach. Synthesis of EDOT functionalized pentaerythritol and preparation of polymers were carried out by R. A. S. and F. G. Electrochemical studies and quartz crystal microbalance experiments were performed by R. A. S. with assistance and analytical input from C. C. BET measurements and PSD calculation were achieved by B. D. and P. L. T. This paper was written by C. C. All authors contributed to the manuscript.

Conflicts of interest

There are no conflicts to declare.

Acknowledgements

This research was funded by the Centre National de la Recherche Scientifique (CNRS-France) and the Agence Nationale de la Recherche (ANR) through the framework of the project HOMERE, grant number ANR-22-CE05-0011.

References

1 J.S. Miller, *Adv. Matter*., 1993, **5**, 671.
2 X. Jia, Y. Ge, L. Shao, C. Wang and G.G. Wallace, *ACS Sustainable Chem. Eng*., 2019, **7**, 14321.
3 A.M. Bryan, L.M. Santino,Y. Lu, S. Acharya and J.M. D'Arcy, *Chem. Mater*., 2016, **28**, 5989.
4 X. Liu, C.-F. Liu, W.-Y. Lai and W. Huang, *Adv. Mater. Technol*., 2020, **5**, 2000154.
5 A.I. Cooper, *Adv. Mater*., 2009, **21**, 1291.
6 K. Amin, N. Ashraf, L. Mao, C.F.J. Faul and Z. Wie, *Nano Energy,* 2021, **85**, 105958.
7 M.A. del Valle, M.A. Gacitúa. E. Hernández, M. Luengo and L.A. Hernández, *Polymers,* 2023, **15**, 1450.
8 Z. Zhou and X.-F. Wu, *J. Power Sources,* 2014, **262**, 44.
9 Y. Shi, L. Peng, Y. Ding, Y. Zhao and G. Yu, *Chem. Soc. Rev*., 2015, **44**, 6684.
10 S. Cho, K.-H. Shin and J. Jang, *ACS Appl. Mater. Interfaces,* 2013, **5**, 9186.
11 C.-F. Lu, S.-F. Liao, K.-H. Wang, C.-T. Chen, C.-Y. Chao and W.-F. Su, *Nanoscale,* 2019, **11**, 20977.
12 J.S. Moore, *Acc. Chem. Res*., 1997, **30**, 402.
13 M. Rose, W. Böhlmann, M. Sabo and S. Kaskel, *Chem. Commun*., 2008, 2462.
14 N.B. McKeown and P.M. Budd, *Macromolecules*, 2010, **43**, 5163.
15 N.B. McKeown and P.M. Budd, *Chem. Soc. Rev*., 2006, **35**, 675.
16 Q. Chen, J.X. Wang, F. Yang, D. Zhou, N. Bian, X.J. Zhang, C.G. Yan and B.H. Han, *J. Mater. Chem*., 2011, **21**, 13554.
17 Q. Chen, M Luo, P. Hammershøj, D. Zhou, Y. Han, B.W. Laursen, C.-G. Yan and B.-H. Han, *J. Am. Chem. Soc*., 2012, **134**, 6084.
18 A.I. Cooper, *Adv. Mater*., 2009, **21**, 1291.
19 A. Ringk, A. Lignie, Y. Hou, H.N. Alshareef and P.M. Beaujuge, *ACS Appl. Mater. Interfaces,* 2016, **8**, 12091.
20 D.F. Zeigler, S.L. Candelaria, K.A. Mazzio, T.R. Martin, E. Uchaker, S.-L. Suraru, L.J. Kang, G. Cao and C.K. Luscombe, *Macromolecules,* 2015, **48**, 5196.
21 M.E. Roberts, D.R. Wheeler, B.B. McKenzie and B.C. Bunker, *J. Mater. Chem*., 2009, **19**, 6977.
22 D.D. Potphode, S.P. Mishra, P. Sivaraman and M. Patri, *Electrochim. Acta,* 2017, **230**, 29.
23 Y. Dai, W. Li, R. Zhao, Q. Huang, N. Xu, F. Yuan and C. Zhang, *Electrochim. Acta,* 2019, **318**, 322.
24 Van At Nguyen and C. Kuss, *J. Electrochem. Soc*., 2020, **167** 065501.
25 T. Darmanin and F. Guittard, *Prog. Polym. Sci*., 2014, **39**, 656.
26 L. Xu, W. Chen, A. Mulchandani and Y. Yan, *Angew. Chem. Int. Ed.*, 2005, **44**, 6009.
27 Y. Han, L.-M. Zhang, Y.-C. Zhao, T. Wang and B.-H. Han, *ACS Appl. Mater. Interfaces,* 2013, **5**, 4166.
28 Y.-C. Zhao, L.-M. Zhang, T Wang and B.-H. Han, *Polym. Chem*., 2014, **5**, 614.
29 M.-Y. Jiang, Q. Wang, Q. Chen, X.-M. Hub, X.-L. Ren, Z.-H. Li and B.-H. Han, *Polymer,* 2013, **54**, 2952.
30 T. Zhu, F. Xie, T. Huang, K. Tian, Z. Wu, H. Yang and L. Li, *ACS Macro Lett.,* 2018, **7**, 1283.
31 M. Ma, L. Guo, D.G. Anderson and R. Langer, *Science,* 2013, **339**, 186.
32 F. Gao, N. Zhang, X. Fang and M. Ma, *ACS Appl. Mater. Interfaces,* 2017, **9**, 5692.
33 M. Li, F. Jiang, J. Yang, Y. Wang, F. Zhao, X. Xu, M. Liu, J. Yan and J. Xu, *ACS Appl. Energy Mater*., 2021, **4**, 12982.
34 D. Zhou, Y. Chen, B. Li, H. Fan, F. Cheng, D. Shanmukaraj, T. Rojo, M. Armand and G. Wang, *Angew. Chem. Int. Ed*., 2018, **57**, 10168.
35 K. Deng, S. Wang, S. Ren, D. Han, M. Xiao and Y. Meng, *J. Power Sources,* 2017, **360**, 98.
36 F. Qi, Z. Xia, R. Sun, X. Sun, X. Xu, W. Wei, S. Wang and G. Sun, *J. Mater. Chem*. A, 2018, **6**, 14170.

37 X. Hu, Y. Luo, X. Wu, J. Niu, M. Tan, Z. Sun and W. Liu, *Mater. Today Energy,* 2022, **27**, 101010.
38 C. Malacrida, A.H. Habibi, S. Gámez-Valenzuela, I. Lenko, P. Simón Marqués, A. Labrunie, J. Grolleau, J.T. López Navarrete, M.C. Ruiz Delgado, C. Cabanetos, P. Blanchard and S. Ludwigs, *ChemElectroChem,* 2019, **6**, 4215.
39 U. Bulut, F. Yilmaz, Y. Yagci, and L. Toppare, *React. Funct. Polym*., 2004, **61**, 63.
40 C. Fave, V. Noel, J. Ghilane, G. Trippé-Allard, H. Randriamahazaka and J.-C. Lacroix, *J. Phys. Chem.* C, 2008, **112**, 18638.
41 V. Stockhausen, G. Trippé-Allard, N.V. Quynh, J. Ghilane and J.-C. Lacroix, *J. Phys. Chem*. C, 2015, **119**, 19218.
42 B. Le Ouay, M. Boudot, T. Kitao, T. Yanagida, S. Kitagawa and T. Uemura, *J. Am. Chem. Soc*., 2016, **138**, 10088.
43 J. Agrisuelas, C. Gabrielli, J.J. García-Jareño, H. Perrot, O. Sel and F. Vicente, *Electrochim. Acta,* 2015, **164**, 21.
44 A. Bund and S. Neudeck, *J. Phys. Chem.* B, 2004, **108**, 17845.
45 A.R. Hillman, S.J. Daisley and S. Bruckenstein, *Electrochem. Commun*., 2007, **9**, 1316.
46 W. Plieth, A. Bund, U. Rammelt, S. Neudeck and LeMinh Duc, *Electrochim. Acta,* 2006, **51**, 2366.
47 V. Noël, H. Randriamahazaka and C. Chevrot, *J. Electroanal. Chem*., 2003, **542**, 33.
48 T.F. Otero, H.-J. Grande and J. Rodríguez, *J. Phys. Chem*. B, 1997, **101**, 3688.
49 T.F. Otero, H.-J. Grande and J. Rodríguez, *Elecrtochim. Acta,* 1996, **41**, 1863.
50 T.F. Otero an M.C. Romero, *J. Phys.: Conf. Ser*., 2008, **127**, 012016.
51 T.F. Otero and I. Boyano, *J. Phys. Chem.* B, 2003,**107**,4269.
52 T.F. Otero and I. Boyano, *J. Phys. Chem*. B, 2003, **107**, 6730;
53 T.F. Otero and M.J. Ariza, *J. Phys. Chem*. B, 2003, **107**, 13954.
54 T.F. Otero, H. Grande and J. Rodríguez, *J. Phys. Chem*. B, 1997, **101**, 8525.
55 H. Grande and T.F. Otero, *J. Phys. Chem*. B, 1998, **102**, 7535.
56 C.P. Andrieux and J.-M. Saveant, *J. Electroanal. Chem.,* 1980, **111**, 377.
57 E. Laviron, *J. Electroanal. Chem*., 1980, **112**, 1.
58 E.F. Dalton, N.A. Surridge, J.C. Jernigan, K.O. Wilbourn, J.S. Facci and R.W. Murray, *Chem. Phys*., 1990, **141**, 143.
59 D.N. Blauch and J.-M. Savéant, *J. Am. Chem. Soc*., 1992, **114**, 3323.
60 A. Akhoury, L. Bromberg and T.A. Hatton, *J. Phys. Chem*. B, 2013, **117**, 333.
61 J. Nightingale, J. Wade, D. Moia, J Nelson and J.-S. Kim, *J. Phys. Chem*. C, 2018, **122**, 29129.
62 J.F. Rubinson and Y.P. Kayinamura, *Chem. Soc. Rev*., 2009, **38**, 3339.
63 C. Gabrielli, O. Haas and H. Takenouti, *J. Appl. Electrochem*., 1987, **17**, 82.
64 M.M. Musiani, *Electrochim. Acta,* 1990, **35**, 1665.
65 X. Ren and P.G. Pickup, *J. Chem. Soc. Faraday Trans*., 1993, **89**, 321.
66 J. Huang, *Electrochim. Acta,* 2018, **281**, 170.
67 T. Jacobsen and K. West, *Electrochim. Acta,* 1995, **40**, 255.